Soft Bending Actuator with Fiber-Jamming Variable Stiffness and Fiber-Optic Proprioception

Joonwon Kang, Sudong Lee, and Yong-Lae Park

***Abstract*— Soft actuators with a function of variable stiffness are beneficial to the improvement of the adaptability of robots, expanding the application areas and environments. We propose a tendon-driven soft bending actuator that can change its stiffness using fiber jamming. The actuator is made of an elastomer tube filled with different types of fiber. The three types of fibers play different roles in maintaining the structure, variable stiffness by jamming, and fiber-optic shape sensing while sharing the same structure and materials, realizing a compact form factor of the entire structure. The stiffness of the actuator can be increased to more than three times its original stiffness by jamming. In addition to jamming, the proposed actuator has a special function of shape sensing that estimates the tip location of the actuator based on image sensing from optical fibers packaged with the jamming fibers. The tip position sensing shows the estimation accuracies with the errors of 3.1%, 3.0%, and 6.7% for the x, y, and z axes, respectively, using feature extraction and a deep neural network. The proposed actuator has two degrees of freedom (i.e., bending on two orthogonal planes) and is controlled by two tendons. When connected in series, multiple actuators form a soft robotic manipulator (i.e., arm), physically compliant or capable of delivering a relatively high force to the target objects.**

I. Introduction

High adaptability has been emphasized as one of the critical requirements in robot design to expand the application areas of robots since an increase in adaptability allows robots to interact with even fragile objects and soft environments and to safely share the same space with humans [1]–[3]. To increase the adaptability, soft actuators have been extensively studied and applied to robots in recent years, realizing inherent mechanical compliance and high degrees of freedom (DoFs) [4], [5]. However, the low stiffness from inherent compliance limits the torque that the robot can generate, confining the application areas. In this case, the function of variable stiffness is one of the solutions that allow both compliance and rigidity in the same structure.

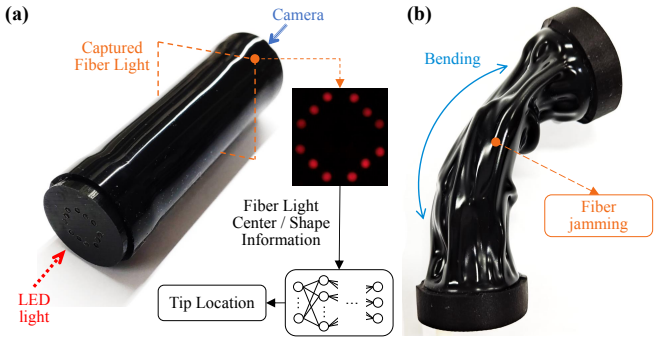

Fig. 1. Variable stiffness bending actuator with fiber jamming. (a) The flow of the sensing mechanism and the initial state without jamming. (b) Proposed actuator with bending and jamming.

A decrease in the stiffness makes the system more interactive with and adaptable to the environments while a stiffness increase allows the system to generate high torque and to control itself with accuracy. There has been research on soft actuators [6]–[8] and their applications [9], [10] by taking advantage of variable stiffness. There are different mechanisms for enabling variable stiffness, such as generation of electrostatic force (e.g., dielectric elastomer actuators, DEAs) [11], [12], change of temperature (e.g., low-melting-point alloys or shape-memory materials) [8], [13], or vacuum jamming actuators [6], [7], [10]. The advantage of DEAs is a fast response time, but they require an extremely high voltage for activation, limiting the application areas due to safety. Although variable stiffness with thermal activation can be implemented in various systems, the response time for heating and cooling is relatively long. The jamming mechanism is an easy and intuitive solution since it only requires negative pressure to change the stiffness.

There are three types of jamming based on the materials and structures: granular jamming, layer jamming, and fiber jamming. Granular jamming uses small particles, such as coffee grounds or glass beads. In this mechanism, the particles act like fluid in a flexible enclosure before jamming and allow the structure to easily conform to the shape of the object in contact [14]–[16]. Although it shows relatively high resistance to compression and shear force when jammed, the structure does not provide a high strength against tensile or bending loads [17]. Layer jamming utilizes the friction

Manuscript received: April 20, 2023; Revised: August 18, 2023; Accepted: September 11, 2023.

This paper was recommended for publication by Editor Cecilia Laschi upon evaluation of the Associate Editor and Reviewers' comments. This work was supported in part by the National Research Foundation (NRF) grants (RS-2023-00208052 and 2021R1A2C2093790) and in part by the Institute of Information & Communications Technology Planning & Evaluation (IITP) grant (2021-0-00896) all funded by the Korea Government (MSIT). *(Joonwon Kang and Sudong Lee contributed equally to this work.) (Corresponding author: Y.-L. Park)*

Joonwon Kang is with the Department of Mechanical Engineering, Seoul National University, Seoul, Korea (e-mail: urgemini@snu.ac.kr).

Sudong Lee was with the Department of Mechanical Engineering, Seoul National University, Seoul, Korea. He is now with the CREATE Lab, Institute of Mechanical Engineering, EPFL, Lausanne, Switzerland (e-mail: sudong.lee@epfl.ch).

Yong-Lae Park is with the Department of Mechanical Engineering; Institute of Advanced Machines and Design (IAMD); Institute of Engineering Research, Seoul National University, Seoul, Korea (e-mail: ylpark@snu.ac.kr).

Digital Object Identifier (DOI): see top of this page.

between planar sheets when the enclosure bag is vacuumed, and it is suitable for light and compact systems [18], [19]. However, the structure allows flexibility only in one direction and increases the stiffness in that direction when jammed [20]. As the name indicates, fiber jamming uses a number of fibers interdigitated in a flexible enclosure. Unlike the other approaches, a structure with a jamming system shows stiffness against compression and tension along the length of the fibers without jamming. For this characteristic, they have been used in various applications, including haptic gloves [17], soft grippers [21], and manipulators [22].

Although the internal compliance of soft actuators enables high adaptability, it complicates modeling and control. Therefore, it is common to add soft sensors to track the state of the soft actuators, usually by wrapping the actuators on the surface [23]. However, this approach makes the system bulky and the fabrication process cumbersome. Therefore, the concept of proprioception directly combined with the actuator is highly beneficial [5], [24], [25].

We propose a tendon-driven soft bending actuator with the functionality of variable stiffness using fiber jamming. The actuator utilizes optical fibers as the filling material for jamming, enabling tip position sensing with an arrangement of light transmission. This approach integrates variable stiffness and proprioception that share the same materials and structures, increasing the efficiency of the design (Fig. 1).

Fiber jamming is one of the widely used methods for variable stiffness, and there have been efforts to increase the structural strength by varying the materials or the arrangement of the fibers [26]–[28]. It has also been used as a means of actuation [29]. However, these approaches do not have any capability of detecting the shapes of the host structures. Although the methods of proprioception for soft robots have recently been proposed using optical waveguides [30]–[32], they have not been combined with jamming structures yet. Researchers have mostly focused on increasing the sensitivity [33] or on improving the fabrication method for effectively integrating the mechanisms of optical sensing into the host structure [34]. We believe this is the first attempt, to the best of our knowledge, to realize the capability of proprioception in a fiber jamming structure, not requiring additional materials and structures for sensing.

The proposed actuator has two active DOFs and is able to increase its stiffness three times the original stiffness by jamming. When connected in series, multiple actuators form an underactuated robotic manipulator. The stiffness of each joint (i.e., each actuator) of the manipulator can be independently controlled by the jamming mechanism. This enables the adaptive interaction of the manipulator with the surroundings. By selectively stiffening the joints of the manipulator, the robot can make itself physically compliant or deliver a relatively high force to the target objects. This is particularly beneficial when the robot needs to simultaneously interact with humans and rigid objects for collaboration tasks.

We used a neural network to estimate the tip location of the manipulator based on the image data from the optical fibers, achieving normalized root mean square errors (NRMSEs) of 3.1%, 3.0%, and 6.7% for the x-, y-, and z-axes, respectively. Since the required feature can be extracted from the captured image with existing algorithms easily, using a simple deep neural network (DNN) model was enough to get the accurate tip position estimation.

The rest of this paper is organized as follows. Section II describes the design, the fabrication process, and the subsystems to operate the actuator. Section III presents analytical models for the stiffness, and Section IV shows the results on the performance of stiffness change and on the sensor calibration. Section V provides potential applications, followed by the contribution of this study and future work in Section VI.

II. Design and Fabrication

A. Design

The proposed bending actuator has two main functions: variable stiffness by fiber jamming and bending angle estimation by optical image sensing. To combine these two different functions into one structure, we used optical fibers with a polyvinyl chloride (PVC) jacket for both functions.

One thick fiber (core diameter: 1 mm) was fixed at the centers of both ends of the structure the same length of the actuator with an initial stiffness even though the actuator was bent ((Fig. 2(a)). 12 medium-thickness fibers (core diameter: 0.75 mm) were then placed around the center fiber and fixed only at the bottom base of the actuator for optical sensing (Fig. 2(a)). They were arranged to form a square shape from the top with three fibers for each, as shown in the cross-section in Fig. 1(a). This arrangement helps the camera located on the other end of the actuator capture at least one light source from each side of the square even though some light sources are missing while the actuator is bent. Moreover, the square arrangement of the optical fibers facilitates asymmetric deformation of the square image detected by the camera when the actuator is bent, making it easy to identify the bending direction.

Lastly, 58 thin fibers (core diameter: 0.5 mm) were placed around the sensing fibers for the stiffening effect by jamming. 20 of them were fixed at the bottom base while the remaining 38 were fixed at the the top base (Fig. 2(b)). When the actuator was not jammed, these fibers easily slide each other, allowing smooth bending of the actuator. However, when jammed, they stick together due to the friction on the PVC jackets and increase the bending stiffness of the actuator [26]. To prevent the jamming fibers from obstructing any light from the sensing fibers, two thin fiber guides with holes were placed around the sensing fibers (Fig. 2(a)). In this way, the jamming fibers maintain their horizontal positions even though they are jammed or bent.

The length of the jamming fibers was set to be as long as possible in the range that their tips do not touch the other side, which maximized the jamming effect while preventing them from buckling during the bending motions. This also helped prevent the interference of the jamming fibers with the sight of the sensing fibers. To reinforce the weakness at the

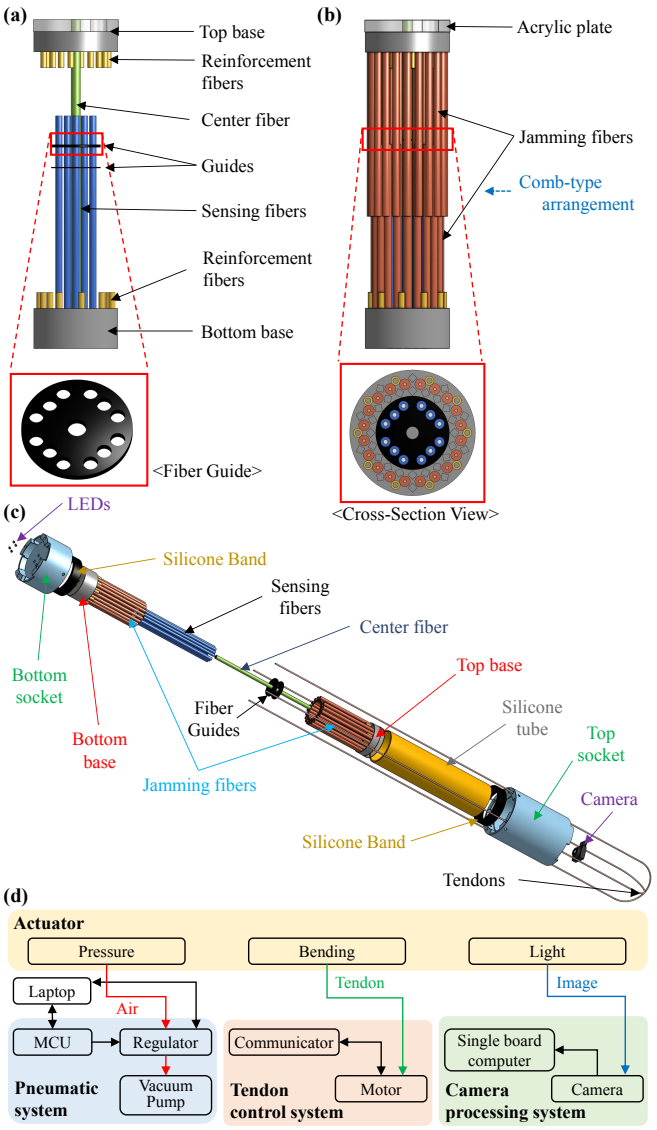

Fig. 2. (a) Arrangement of a center fiber, sensing fibers, and guides. (b) Configuration after placing sensing fibers. (c) The expansion view of a whole actuator with sockets, tendons, and optical components. (d) Actuator system configuration with three subsystems.

ends of the actuator, 20 short fibers (length of 2.0 mm), called reinforcement fibers, were added to the remaining space of each end (Fig. 2(b)).

A rigid socket (radius: 16.7 mm) was attached to each end of the actuator to implement tendon-driven actuation and light sensing. One socket contains four light-emitting diodes (LEDs) and an optical diffuser for making uniform light distribution. The light passes only through the 12 sensing fibers. The other socket has a miniature complementary metal–oxide–semiconductor (CMOS) camera that was able to capture the light from the sensing fibers through a transparent acrylic plate. After attaching the sockets, the length of the actuator became 82 mm.

Multiple actuators can be connected in series by mating the teeth of the sockets, making a soft manipulator. The manipulator is actuated by two tendons that pass through the holes in the sockets. The ends of the tendons were fixed to the final socket. Motors with pulleys were located in the middle of each tendon, controlling the highly adaptive movement of the manipulator with two tendons.

B. Fabrication

Fibers are then cut by laser (Flexx Speedy 300, Trotec) to the dimensions determined in Section II-A. The center and the sensing fibers are fixed to the top base, fabricated by a 3D printer (Objet 30 Prime, Stratasys) using an adhesive (Loctite 401, Henkel). Two fiber guides are attached to the center fiber and wrap the sensing fibers around. The guides made of PVC films with a thickness of 0.2 mm are placed 7 mm and 12 mm below the end of the sensing fibers, respectively. The upper guide is reinforced by stacking three PVC films.

The bottom base is fabricated by attaching a transparent acrylic plate to a 3D-printed part. In order to prevent optical noise by light reflection, we polished the inner surface of the 3D printed part and the lower surface of the sensing fibers stuck to the bottom base with sandpaper, making the reflection diffused. The inner surface of the 3D-printed part is also coated with matte nail polish. After that, the jamming fibers are affixed to the bases using the adhesive, and both bases are connected through the center fiber. The configuration of the assembled part is shown in Fig. 2(a).

The assembled part is enveloped by a thin silicone tube, made of silicone elastomer (Dragon Skin 30, Smooth-On) in a similar way to the method introduced by Brancadoro *et al*. [27]. A black pigment is added to the silicone in a weight ratio of 3% to block the light from the outside of the tube. Silicone bands with the same elastomer are fitted over the tube on both bases, sealing the actuator.

We place the top and the bottom sockets fabricated by a 3D printer (Mark Two, Markforged) on silicone bands and fix them with bolts. Four surface mounted light emitting diodes (LEDs) are attached to the bottom socket with an optical diffuser inside. The optical diffuser is made by attaching a diffusing film on both sides of a 5 mm acrylic plate. The top socket is equipped with a camera (Raspberry Camera Module 2 Noir) aligned with the center hole. The entire structure of the proposed actuator is shown in Fig. 2(c).

C. System

The system for operating the manipulator with the actuators connected in series requires three subsystems: the pneumatic system, the tendon control system, and the camera processing system (Fig. 2(d)). The pneumatic system controls the pressure of the actuator for jamming by using a vacuum pump with valves and a regulator (ITV0091-2L, SMC Pneumatics). The tendon control system controls the positions of the two tendons by operating two motors (XH430-W350-R, Robotis) with pulleys. The camera processing system includes a camera (Raspberry Pi Camera Module 2 NoIR, Raspberry Pi Foundation) and a single-board computer (Raspberry Pi 4 Model B, Raspberry Pi Foundation) to record the captured video.

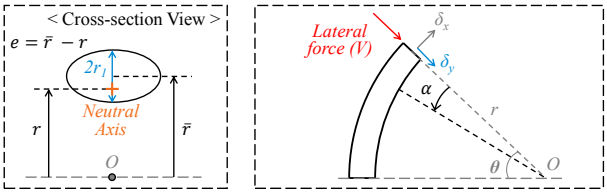

Fig. 3. Cross-section and bent configuration of the actuator under the vertical force applied on the tip.

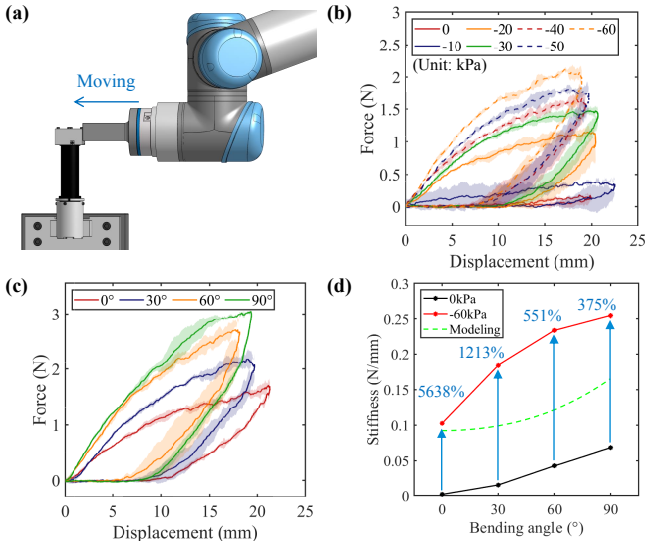

Fig. 4. (a) Experiment setup for measuring tip force of the actuator. Measured tip force versus displacement (b) under various jamming pressures without bending and (c) under various bending angles with the jamming pressure of -60 kPa applied. (d) Stiffness of the actuator. Experimental results are shown in solid lines and the result calculated by Eqn. (6) under the assumption of the jammed state is shown in a dotted line.

III. Stiffness Modeling

When the actuator is jammed, the stiffness of the actuator changes according to the structural form, such as the bending angle. Fig. 3 shows the configuration of the actuator at the arbitrary bending angle. If the radius of curvature is large enough to be greater than ten times the depth, the stress distribution of the cross-section can be found with linear approximation across the depth [35]. This approximation can be applied to our design when the bending angle is less than 17.5°. When a force is applied to the tip perpendicular to the tangent of the bending arc, the complementary energy of the flexure is

$$U_f = \int_0^\theta \frac{(Vr\sin\alpha)^2}{2EI} r d\alpha \tag{1}$$

where θ is the bending angle, E is the modulus of elasticity, I is the moment of inertia, V is the lateral force, r is the radius of curvature, and α is the angular position from the tip [36]. (The formula with the applied force including horizontal direction can be found in [35].) According to Castigliano's second theorem, the deflection δ_y is

$$\delta_y = \frac{\partial U_f}{\partial V} = \frac{Vr^3(\theta - \sin\theta\cos\theta)}{2EI} \tag{2}$$

and the stiffness K is

$$K = \frac{V}{\delta_y} = \frac{2EI\theta^3}{l^3(\theta - \sin\theta\cos\theta)} \tag{3}$$

where the bend radius r is l/θ.

If the radius of curvature is small enough to be less than ten times the depth, the stress distribution of the cross-section is not linear across the depth [35]. Furthermore, the deflection is affected by the shear stresses due to the vertical force and the circumferential normal stresses due to the axial force. The complementary energy of the flexure is

$$U_f = \int_0^\theta \frac{M_x^2}{2AEe} dx + \int_0^\theta \frac{FV_x^2 r}{2AG} dx + \int_0^\theta \frac{N_x^2 r}{2AE} dx - \int_0^\theta \frac{M_x N_x}{AE} dx \tag{4}$$

where M_x, V_x, N_x, A, G, e, and F are the moment, the shear force, the axial force, the area, the shear modulus of elasticity, the distance from the centroidal axis to the neutral axis, and the factor depending on the form of the cross-section, respectively [35]. According to Castigliano's second theorem, in the same way in Eqn. (2), the deflection δ_y becomes

$$\delta_y = \left(\frac{Vr^2 - Vre}{2AEe}\right)(\theta - \sin\theta\cos\theta) + \frac{FVr}{2AG}(\theta + \sin\theta\cos\theta) \tag{5}$$

where M_x is $Vr\sin x$, V_x is $V\cos x$, and N_x is $V\sin x$. r is l/θ, and e is $r_1^2/4R$ where r_1 is the length of a semi-minor axis assuming that the shape of the cross-section is an ellipse (Fig. 3). Therefore, K is as follows

$$K = \left[\frac{l}{2AE\theta}\left(\frac{4l^2}{r_1^2\theta^2} - 1\right)(\theta - \sin\theta\cos\theta) + \frac{Fl}{2AG\theta}(\theta + \sin\theta\cos\theta)\right]^{-1}. \tag{6}$$

For Eqn. (6), the first term is the dominant term considering the relative magnitude of the coefficients and this term is a consistently increasing function of θ as Eqn. (3). Therefore, the stiffness of the actuator is expected to increase as the bending angle increases.

IV. Characterization

A. Stiffness

The stiffness of the actuator changes with the magnitude of the negative pressure and the bending angle. We calibrated the stiffness and the tip force through experiments in which a commercial robotic arm applied forces to the tip perpendicular to the tangent of the bending arc.

1) Setup: The tip force generated by the actuator was measured by a loadcell (RFT60-HA01, Robotous) that was connected to the end effector of the robotic arm (UR5e, Universal Robotics). To maintain the surface contact between the bottom socket of the actuator and the loadcell, a rectangular indenter was attached to the loadcell. Furthermore, the bottom socket was replaced with one with a flat side for stable contact with the indenter. The top socket was embedded in 3D-printed parts holding the motors, and the

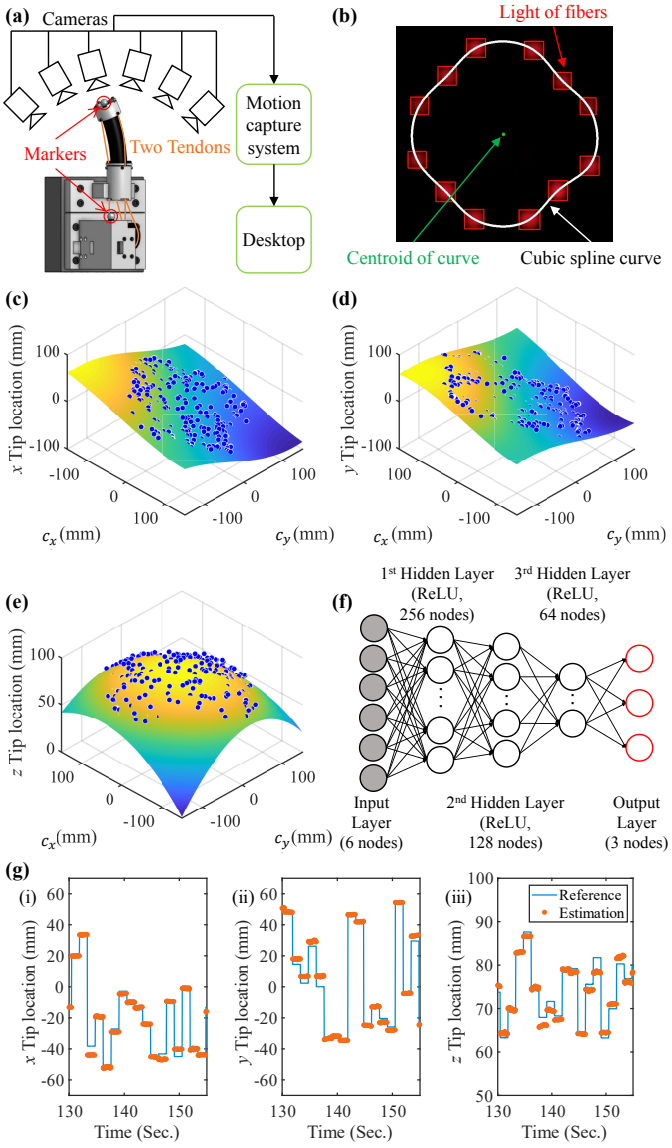

Fig. 5. (a) Experiment setup for the sensor calibration. (b) Preprocessing of the picture to characterize the fiber arrangement. The surface fitting results of the tip location of (c) x, (d) y, and (e) z-axis. (f) The structure of the DNN model for tip location estimation (Optimizer: Adam, Learning Rate: 0.001, Batch Size: 256). (g) Estimation results of the DNN for the tip location of (i) x, (ii) y, and (iii) z-axis.

entire assembly was fixed on an optical table. To eliminate the effect of tendons on the stiffness during the experiment, the torques of the motors for driving the tendons were set to zero after creating a desired bending angle. The negative pressure was controlled by the vacuum pump and the regulator.

2) Result: Fig. 4(b) shows the measured tip forces for the displacement with varied negative pressures, and the slope of each curve indicates the stiffness of the actuator. As the magnitude of the negative pressure increases, the silicone tube tightens the fibers more strongly and the friction between the fibers increases, reinforcing the jamming effect. Therefore, it is confirmed that the slope and the stiffness increase as the inside of the actuator approaches the vacuum state (Fig. 4(b) and (d)).

Fig. 4(c) shows the measured tip forces for four bending angles (θ) when the pressure inside the actuator was -60 kPa. It is demonstrated that the stiffness of the jammed actuator can be changed by the structural form, such as the bending angle, in Section III-B. The stiffness increases as the bending increases (Fig. 4(c) and (d)), which is the same trend as Eqn. (3), (6). However, there exist differences in the exact value and the convexity between the modeling and the experiment results.

B. Sensor

The proposed actuator has two DoFs that are controlled by two pairs of tendons and two motors. Each pair was connected to one of the two motors through a pulley for bidirectional motions. Although the changes in the length of the tendons can be obtained using the encoders of the motors, it is difficult to estimate the tip positions of the actuator only with the encoder values due to the structural compliance of the actuator. Therefore, the tip positions need to be detected with an additional method. For the simplicity and practical applications of the proposed system, we implemented the concept of proprioception using integrated optical sensing, which made it possible to detect the tip position without using any external sensing devices. The model for estimating the tip position was trained with the optical sensor data and validated using the measurements from a commercial motion capture system considered to be ground truth.

1) Setup and Processing: A motion capture system with six cameras (Prime$^{\text{X}}$ 13W, Optitrack) was used to acquire the reference tip positions of the actuator while the actuator was moving. The three-dimensional (3D) tip location was traced using two markers attached to the tip and the fixed base frame. We collected training (predetermined 324 points) and test (randomly selected 84 points) data sets to estimate the tip positions and to validate the estimation results, respectively. The reason for using the predetermined points rather than a number of random points collected while the actuator makes arbitrary motions is to prevent unintended bias during the training process, by securing a uniform point distribution in the data set. Although the actuator can be bent up to approximately 120° mechanically, the functional workspace is limited by the range of sensing. Since the optical sensing is not functional if the camera loses more than two red dots on the same side from its sight, the data in the training and the test sets were acquired within the bending angle of 80°.

The captured images were post-processed by the open-source computer vision library (OpenCV) to find the locations and the areas of the light from the sensing fibers. To characterize the state of the entire fibers even when the camera missed the lights from some of the fibers, the cubic spline curve was made using the detected lights (Fig. 5(b)).

2) Result: The tip position was estimated by the centroid position of the cubic spline curve. We defined the position of the centroid as (c_x, c_y). The data of (c_x, c_y) were then fitted to the x, y, and z values of the tip, one by one, by cubic polynomial surfaces. The result of surface fitting obtained

TABLE I

SENSOR CALIBRATION RESULTS

Tip location	Surface fitting			Machine learning		
	x	y	z	x	y	z
RMSE (mm)	3.2	2.9	2.5	2.9	2.8	2.0
NRMSE (%)	3.4	3.1	8.3	3.1	3.0	6.7

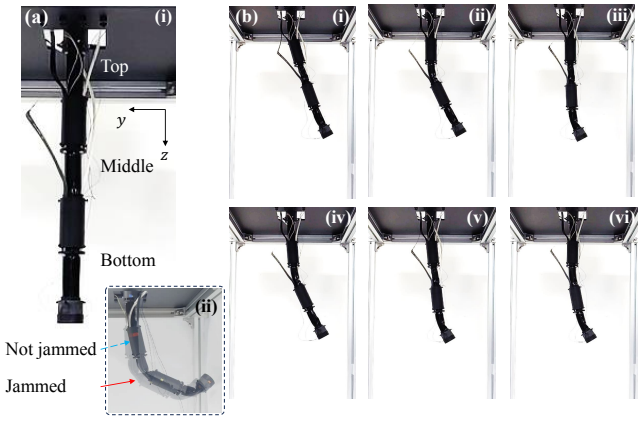

Fig. 6. (a) Manipulator setup. (b) Six different configurations are made by varying modes of the manipulator: the jamming state of the mode corresponding to each configuration is tabulated in Table II.

from the train data set confirms that there exists a correlation between the tip location and the centroid position of the cubic spline curve (Fig. 5(c)). Since the tip location and the centroid position are determined by bending. The blue points represent the obtained data during the experiment, and the color of the fitted surfaces represents the value of the estimated tip location, showing a higher value as the color becomes close to yellow. Table I summarizes the estimation results using the test data set by calculating the root-mean-square error (RMSE) and the normalized RMSE (NRMSE). The NRMSE values were calculated by dividing the RMSE values in each direction with the range of the position coordinate in each direction and taking a percentage.

The tip position of the soft actuator is expressed with a nonlinear function, and it is difficult to find an analytical solution. Therefore, we trained a DNN model to enhance the estimation performance using the train data set through Pytorch. The DNN model consists of five fully-connected (FC) layers: the input layer, three hidden layers, and the output layer. Along with the centroid position of the cubic spline curve, the information on the shape of the spline curve is added as the input. The shape is represented by the area of each quadrant about the curve centroid. Therefore, the input layer includes six nodes, and the output layer has three nodes to predict the tip position with x, y, and z values. The network is shown in Fig. 5(f). Fig. 5(g) and Table I show the estimation results using the test data set.

V. APPLICATION

A soft robotic manipulator was built by connecting multiple actuators in series, constructing an underactuated arm. The manipulator requires only two tendons along the entire length of its body for 3D motions. However, the stiffness

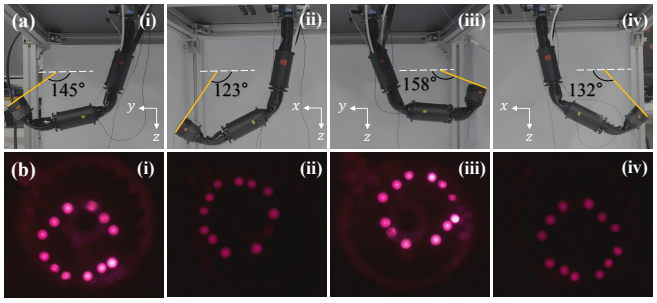

Fig. 7. (a) Maximum bending angle measured in four directions. (b) Captured image by the camera in the middle actuator in each direction under the maximum bending angle.

TABLE II

MODES OF THE MANIPULATOR WITH THREE ACTUATORS

Mode	Top - Middle - Bottom	Mode	Top - Middle - Bottom
1	Free - Jammed - Jammed	4	Jammed - Free - Free
2	Jammed - Free - Jammed	5	Free - Jammed - Free
3	Jammed - Jammed - Free	6	Free - Free - Jammed

of each actuator can be controlled independently. Some actuators maintain their postures by increasing the stiffness through jamming, while the others move freely based on the structural compliance. Depending on the jamming state of each actuator, different motions and shapes of the manipulator can be created even under the same motor input. Furthermore, combinations of different jamming states enable adaptive manipulation depending on the environment.

A. Manipulator Setup

The manipulator was constructed using three actuators and three rigid links connected alternatively in series and hung on an aluminum frame (Fig. 6(a)-i). The three actuators become the flexible joints that connect rigid links when unjammed (Fig. 6(a)-i). If the jamming is applied, the undesired bending motion of the actuator can be restricted. The configurations when the top actuator is not jammed and jammed are compared in Fig. 6(a)-ii). Although the top actuator has to resist a significant bending moment, it is not bent when jamming is applied. Instead, the other actuators bend more compared to the state when all actuators are left unjammed.

Fig. 7 shows the result of the maximum bending angle test in four directions. The maximum bending angle is defined as the first angle when the tendon in the opposite applies tension to the actuators by touching them. It is distributed between 120° to 160°. In all maximum bending cases, the sensing mechanism in the middle actuator worked without losing a single sensing node.

B. Operation Modes

Adaptive manipulation is available by independently controlling the jamming pressure of each actuator. In particular, six unique modes exist depending on the jamming state of each actuator (Table II). Even under the same motor input, the shape of the manipulator may be different depending on the jamming mode (Fig. 6(b)). In this demonstration, the motion was restricted on the y-z plane, only controlling the motor for the roll motion to clearly show the difference

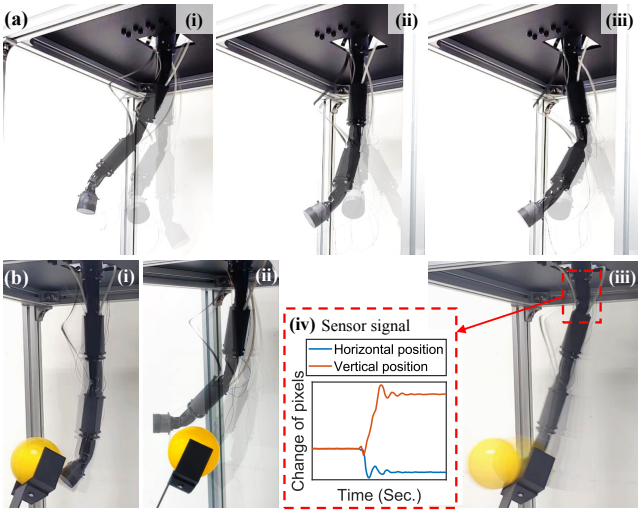

Fig. 8. (a) Different postures of the manipulator, made by varying the mode sequence with the same motor input sequence. (b) Adaptive interaction of the manipulator with the ball for (i) contact with compliance, (ii) evasion, (iii) contact with an impact. (iv) The graph shows the amount of change in the centroid of the cubic spline curve in the top actuator.

between the modes. The manipulator was able to achieve relatively complex configurations by changing the modes during manipulation (Fig. 8(a)).

C. Adaptive Interaction with Object

It is unavoidable for manipulators to be involved with collisions unless they are operated with isolation, and compliance helps protect both the manipulator and the object for interaction. On the other hand, the manipulator should be able to generate enough force to manipulate the object with dexterity. The proposed manipulator meets these requirements by utilizing the different jamming modes. The performance of adaptive interaction was tested through experiments with a ball fixed on a rigid holder.

When compliance is desired, the manipulator behaves like an underactuated arm, making adaptive interactions with the environment. Without jamming any actuators, the manipulator reaches and touches the ball but does not interrupt its position (Fig. 8(b)-i), minimizing the damage by the collision. When the end-effector collides with an unexpected object while operating a task, the manipulator can detour around it and reach the target point by dynamically changing the mode (Fig. 8(b)-ii). On the other hand, the manipulator can stiffen the joints and generate a large force enough to move the target object. By jamming only the middle and the bottom actuators with -60 kPa, the manipulator was able to reach and push the ball away (Fig. 8(b)-iii). The motion of the manipulator can be tracked by the embedded optical sensing (Fig. 8(b)-iv).

VI. Discussion and Future Work

In this paper, we proposed a bending actuator that has the capabilities of actively changing its stiffness and of sensing its deformation shape (i.e., tip location). The use of optical fibers for both jamming and sensing makes the physical system simple and compact. The variable stiffness mechanism makes a robot made of the proposed actuators safely interact with target objects by increasing ~~the~~ environmental adaptability. In addition, the underactuated arm made of the proposed actuators connected in series demonstrated the capability of independently controlling the stiffness in each joint for different purposes. These properties allow the manipulator to create complex postures and to adaptively interact with the environment. Finally, the actuator detects its own shape using the embedded fiber-optic sensing mechanism, estimating the tip location, which makes the system compact and simple. The estimation process for shape sensing only requires a simple DNN structure with six inputs at each frame while achieving relatively high accuracies, which was possible through the feature extraction from the spline curve of the detected light points. The result of position sensing showed a potential of proprioception integrated with the host robot in terms of practicality and cost, since it does not require any expensive equipment with a high-power processing unit, such as motion capture systems.

There is room for further improvements. The jamming performance can be improved by increasing the friction and the density of the fibers. It can benefit from the stiffness modeling customized for our actuator. In Fig. 4(b), the modeling and the experimental data are on the same scale and the stiffness increases as the bending angle increases. However, there were differences in the exact value and the convexity of the graph. The differences are due to the cross-section shape which has vacancy inside because of sensing fibers, and the change in parameters as the actuator bends. More accurate modeling that considers these aspects could help find the optimal design parameters. Another area of future work would be improving the performance of the sensing mechanism. Since the DNN for the optical sensing was trained with a general gradient descent algorithm in our system, the accuracy can be improved with analytical modeling, such as a governing equation for the bending of the actuator, to constrain the optimization problem.

In the case of the soft robotic manipulator, it requires additional validation to utilize proprioception. For characterization, the DNN was trained to predict the tip position using the information from the sensing fibers under the assumption that the actuator followed a constant curvature (CC) model without twisting. Ideally, the model of the entire system made of multiple actuators connected in series can be treated as a CC model with a serial connection. Therefore, the tip position of the manipulator can be found through forward dynamics using transformation matrices derived from the tip position of each actuator. However, it was observed that the load applied by the weight alters the bending motion, requiring validation or a new training method for the manipulator.

Making the actuator multi-modal is another interesting direction for future work. The purpose of the introduced sensing mechanism is to estimate the tip position. Considering that the advantages of soft robots are more pronounced when interacting with the environments, the actuator will be more useful if the external force can be measured, which would be possible by embedding soft tactile sensors [37]–

[39] on the outer surface of the actuator. With the multi-modal function, the active stiffness control which ensures safety would be possible. Also, if the neural network is trained with the output of the additional sensors as well, we can expect the estimation result of the tip position to be more accurate.

ACKNOWLEDGMENTS

The authors would like to thank Dr. Sukho Song for his technical feedback on this work.

REFERENCES

[1] G. M. Whitesides, "Soft robotics," *Angew. Chem. Int. Ed.*, vol. 57, no. 16, pp. 4258–4273, 2018.

[2] D. Rus and M. T. Tolley, "Design, fabrication and control of soft robots," *Nature*, vol. 521, no. 7553, pp. 467–475, 2015.

[3] C. Laschi, B. Mazzolai, and M. Cianchetti, "Soft robotics: Technologies and systems pushing the boundaries of robot abilities," *Sci. Rob.*, vol. 1, no. 1, p. eaah3690, 2016.

[4] G. Shin, Y. Choi, B. Jeon, I. Choi, S. Song, and Y.-L. Park, "Soft electromagnetic artificial muscles using high-density liquid-metal solenoid coils and bistable stretchable magnetic housings," *Adv. Funct. Mater*, p. 2302895, 2023.

[5] J. Wirekoh, L. Valle, N. Pol, and Y.-L. Park, "Sensorized, flat, pneumatic artificial muscle embedded with biomimetic microfluidic sensors for proprioceptive feedback," *Soft Rob.*, vol. 6, no. 6, pp. 768–777, 2019.

[6] F.-Y. Xu, F.-Y. Jiang, Q.-S. Jiang, and Y.-X. Lu, "Soft actuator model for a soft robot with variable stiffness by coupling pneumatic structure and jamming mechanism," *IEEE Access*, vol. 8, pp. 26 356–26 371, 2020.

[7] M. Ibrahimi, L. Paternò, L. Ricotti, and A. Menciassi, "A layer jamming actuator for tunable stiffness and shape-changing devices," *Soft Rob.*, vol. 8, no. 1, pp. 85–96, 2021.

[8] J. Shintake, B. Schubert, S. Rosset, H. Shea, and D. Floreano, "Variable stiffness actuator for soft robotics using dielectric elastomer and low-melting-point alloy," in *IEEE/RSJ Int. Conf. Intell. Rob. Syst.*, 2015, pp. 1097–1102.

[9] L. A. Al Abeach, S. Nefti-Meziani, and S. Davis, "Design of a variable stiffness soft dexterous gripper," *Soft Rob.*, vol. 4, no. 3, pp. 274–284, 2017.

[10] J.-y. Nagase, S. Wakimoto, T. Satoh, N. Saga, and K. Suzumori, "Design of a variable-stiffness robotic hand using pneumatic soft rubber actuators," *Smart Mater. Struct.*, vol. 20, no. 10, p. 105015, 2011.

[11] H. Imamura, K. Kadooka, and M. Taya, "A variable stiffness dielectric elastomer actuator based on electrostatic chucking," *Soft Matter*, vol. 13, no. 18, pp. 3440–3448, 2017.

[12] W.-B. Li, W.-M. Zhang, H.-X. Zou, Z.-K. Peng, and G. Meng, "A novel variable stiffness mechanism for dielectric elastomer actuators," *Smart Mater. Struct.*, vol. 26, no. 8, p. 085033, 2017.

[13] T. P. Chenal, J. C. Case, J. Paik, and R. K. Kramer, "Variable stiffness fabrics with embedded shape memory materials for wearable applications," in *IEEE/RSJ Int. Conf. Intell. Rob. Syst.*, 2014, pp. 2827–2831.

[14] P. S. Wellborn, N. P. Dillon, P. T. Russell, and R. J. Webster, "Coffee: the key to safer image-guided surgery—a granular jamming cap for non-invasive, rigid fixation of fiducial markers to the patient," *Int. J. Comput. Assisted Radiol. Surg.*, vol. 12, no. 6, pp. 1069–1077, 2017.

[15] J. R. Amend, E. Brown, N. Rodenberg, H. M. Jaeger, and H. Lipson, "A positive pressure universal gripper based on the jamming of granular material," *IEEE Trans. Rob.*, vol. 28, no. 2, pp. 341–350, 2012.

[16] S. Chopra, M. T. Tolley, and N. Gravish, "Granular jamming feet enable improved foot-ground interactions for robot mobility on deformable ground," *IEEE Rob. Autom. Lett.*, vol. 5, no. 3, pp. 3975–3981, 2020.

[17] S. Jadhav, M. R. A. Majit, B. Shih, J. P. Schulze, and M. T. Tolley, "Variable stiffness devices using fiber jamming for application in soft robotics and wearable haptics," *Soft Rob.*, vol. 9, no. 1, pp. 173–186, 2022.

[18] J. Kwon, I. Choi, M. Park, J. Moon, B. Jeong, P. Pathak, J. Ahn, and Y.-L. Park, "Selectively stiffening garments enabled by cellular composites," *Adv. Mater. Technol.*, vol. 7, no. 9, p. 2101543, 2022.

[19] Y.-J. Kim, S. Cheng, S. Kim, and K. Iagnemma, "A novel layer jamming mechanism with tunable stiffness capability for minimally invasive surgery," *IEEE Trans. Rob.*, vol. 29, no. 4, pp. 1031–1042, 2013.

[20] S. G. Fitzgerald, G. W. Delaney, and D. Howard, "A review of jamming actuation in soft robotics," *Actuators*, vol. 9, no. 4, p. 104, 2020.

[21] B. Yang, R. Baines, D. Shah, S. Patiballa, E. Thomas, M. Venkadesan, and R. Kramer-Bottiglio, "Reprogrammable soft actuation and shape-shifting via tensile jamming," *Sci. Adv.*, vol. 7, no. 40, p. eabh2073, 2021.

[22] M. Brancadoro, M. Manti, F. Grani, S. Tognarelli, A. Menciassi, and M. Cianchetti, "Toward a variable stiffness surgical manipulator based on fiber jamming transition," *Front. Rob. AI*, vol. 6, p. 12, 2019.

[23] B. K. Johnson, V. Sundaram, M. Naris, E. Acome, K. Ly, N. Correll, C. Keplinger, J. S. Humbert, and M. E. Rentschler, "Identification and control of a nonlinear soft actuator and sensor system," *IEEE Rob. Autom. Lett.*, vol. 5, no. 3, pp. 3783–3790, 2020.

[24] R. L. Truby, C. Della Santina, and D. Rus, "Distributed proprioception of 3D configuration in soft, sensorized robots via deep learning," *IEEE Rob. Autom. Lett.*, vol. 5, no. 2, pp. 3299–3306, 2020.

[25] M. Park, B. Jeong, and Y.-L. Park, "Hybrid system analysis and control of a soft robotic gripper with embedded proprioceptive sensing for enhanced gripping performance," *Adv. Intell. Syst.*, vol. 3, no. 3, p. 2000061, 2021.

[26] M. Brancadoro, M. Manti, S. Tognarelli, and M. Cianchetti, "Preliminary experimental study on variable stiffness structures based on fiber jamming for soft robots," in *IEEE Int. Conf. Soft Rob. (RoboSoft)*, 2018, pp. 258–263.

[27] ——, "Fiber jamming transition as a stiffening mechanism for soft robotics," *Soft Rob.*, vol. 7, no. 6, pp. 663–674, 2020.

[28] L.-J. Gai, J. Huang, and X. Zong, "Stiffness-tunable soft bellows actuators by cross-fiber jamming effect for robust grasping," *IEEE/ASME Trans. Mechatron.*, 2023.

[29] L. Arleo, L. Lorenzon, and M. Cianchetti, "Variable stiffness linear actuator based on differential drive fiber jamming," *IEEE Trans. Rob.*, 2023.

[30] I. Van Meerbeek, C. De Sa, and R. Shepherd, "Soft optoelectronic sensory foams with proprioception," *Sci. Rob.*, vol. 3, no. 24, p. eaau2489, 2018.

[31] J. Jung, M. Park, D. Kim, and Y.-L. Park, "Optically sensorized elastomer air chamber for proprioceptive sensing of soft pneumatic actuators," *IEEE Rob. Autom. Lett.*, vol. 5, no. 2, pp. 2333–2340, 2020.

[32] C. To, T. Hellebrekers, J. Jung, S. J. Yoon, and Y.-L. Park, "A soft optical waveguide coupled with fiber optics for dynamic pressure and strain sensing," *IEEE Rob. Autom. Lett.*, vol. 3, no. 4, pp. 3216–3223, 2019.

[33] B. Wange, W. Guo, S. Feng, Y. Hongdong, F. Wan, and C. Song, "Volumetrically enhanced soft actuator with proprioceptive sensing," *IEEE Rob. Autom. Lett.*, vol. 6, no. 3, pp. 5284–5291, 2021.

[34] B. Jamil, G. Yoo, Y. Choi, and H. Rodrigue, "Proprioceptive soft pneumatic gripper for extreme environments using hybrid optical fibers," *IEEE Rob. Autom. Lett.*, vol. 6, no. 4, pp. 8694–8701, 2021.

[35] W. C. Young and R. G. Budynas, *Roark's formulas for stress and strain*, 7th ed. New York, NY, USA: McGraw Hill, 2001.

[36] R. C. Hibbeler, *Mechanics of Materials*, 8th ed. Upper Saddle River, NJ, USA: Pearson Prentice Hall, 2011.

[37] Y.-L. Park, B.-R. Chen, and R. J. Wood, "Design and fabrication of soft artificial skin using embedded microchannels and liquid conductors," *IEEE Sens. J.*, vol. 12, no. 8, pp. 2711–2718, 2012.

[38] S. J. Yoon, M. Choi, B. Jeong, and Y.-L. Park, "Elongatable gripper fingers with integrated stretchable tactile sensors for underactuated grasping and dexterous manipulation," *IEEE Trans. Rob.*, vol. 38, no. 4, pp. 2179–2193, 2022.

[39] J. Kim, S. Kim, and Y.-L. Park, "Single-input single-output multi-touch soft sensor systems using band-pass filters," *npj Flexible Electron.*, vol. 6, no. 1, p. 65, 2022.